

Stress Distribution Behavior in Single-Lap Adhesively Bonded Beams

X. He¹ and Y. Wang²

Innovative Manufacturing Research Center, Faculty of Mechanical and Electrical Engineering, Kunming University of Science and Technology, Kunming, China

¹ hhxccc@yahoo.co.uk

² bsdyuqi@126.com

УДК 539.4

Распределение напряжений в балках, адгезионно соединенных внахлестку

Кс. Хи, Ю. Ванг

Исследовательский центр инновационного производства, Факультет машиностроения и электротехники, Куньминский университет науки и технологии, Куньмин, Китай

С помощью трехмерного метода конечных элементов исследовалось распределение напряжений вдоль неразрезных балок, адгезионно соединенных внахлестку. Для четырех типичных характеристик связующих материалов получены распределения напряжений в соединенном сечении. Результаты исследований показали, что для компонент напряжений S_{11} , S_{22} , S_{12} и S_{13} имеет место сингулярность напряжений на нижней и верхней границах балки. Чем выше граничные значения твердости связующих материалов, тем меньше значения напряжений разрыва в склеиваемых и связующих материалах на границах. Полученные результаты свидетельствуют о том, что в неразрезных балках, соединенных внахлестку, составляющие нормальных S_{11} , S_{33} и касательных S_{13} напряжений доминируют среди составляющих полей напряжений, причем напряжение S_{11} является самым высоким, а напряжение S_{33} – самым опасным, поскольку связано с напряжением отрыва. Результаты численных исследований показали, что коэффициенты концентрации напряжений варьируются как для разных компонент напряжений, так и для разных связующих материалов, являясь практически одинаковыми для двух концов связующего сечения.

Ключевые слова: балка, соединенная внахлестку, распределение напряжений, конечноэлементный анализ, адгезионность, сингулярность напряжений.

Introduction. Adhesive bonding is becoming a widespread candidate technique for joining light-weight structural components. Consequently the static and dynamic behavior of these joints has been the subject of a considerable amount of experimental and numerical studies [1–6]. However, most investigations of the stress distribution in single-lap adhesively bonded beams have focused solely on the adhesive layers. There has been no work found which considered the stress distribution over the entire single-lap adhesively bonded beams including the adherends and the adhesive layer. Although the adhesive layer is the critical part of a single-lap adhesively bonded beam, it is very important to know the stress distributions not only in the adhesive layer, but also in the adherends and at the adherend–adhesive interfaces.

In the present work, the stress distribution along the total single-lap adhesively bonded beam has been investigated using the 3D finite element (FE) method. Specifically, FE solutions of the stress distributions in the bonded section have been obtained for four typical characteristics of adhesives.

1. Configuration and Properties of Adhesively Bonded Beams with Different Adhesives.

1.1. **Configuration and Material Properties.** The single-lap adhesively bonded beam studied in the present work is shown in Fig. 1. The two adherends used were aluminium alloy plates of the following dimensions: 200 mm long, 25 mm wide, and 4 mm thick. The boundary conditions are also shown in Fig. 1. A distributed load of 1000 N is applied at the right end face of the upper adherend in the x -direction. The free end of the upper adherend is restrained in the z -direction, that is, there is zero displacement in the z -direction.

In order to make the description of the different parts of the beam clear, the beam is subdivided as shown in Fig. 1: point A corresponds to the clamped end of the lower adherend ($x = 0$); point B – to the left free end of the bonded section and the upper adherend ($x = 0.175$ m); point C – to the right free end of the bonded section and the lower adherend ($x = 0.2$ m); point D – to free or simply supported end of the upper adherend ($x = 0.375$ m).

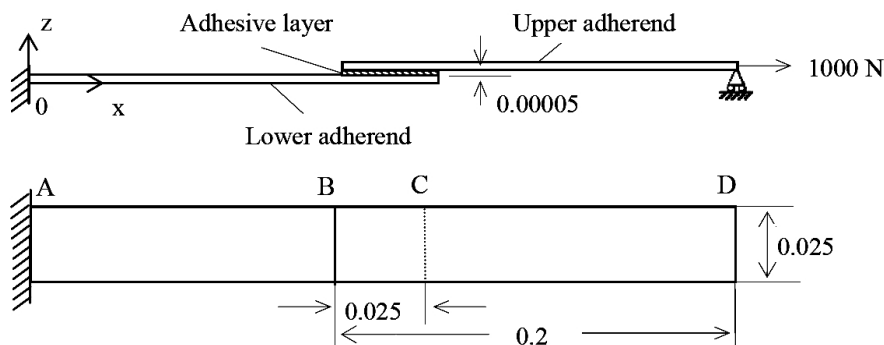


Fig. 1. A single-lap adhesively bonded beam.

The range of adhesive properties covers the mechanical properties of various types of structural adhesives including rubbers, elastomers, epoxies and ceramic glues as illustrated in Fig. 2. In this figure, the Young modulus and Poisson’s ratio are plotted against the hardness of materials. The three different regions of viscoelastic behaviour and some types of adhesives that fall into these categories are shown in Fig. 2.

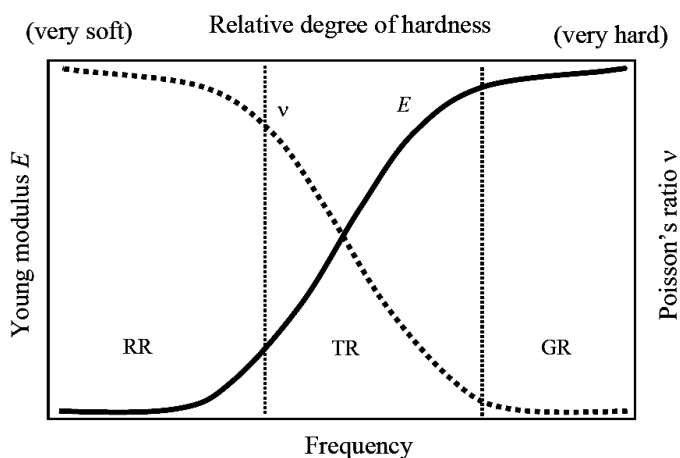


Fig. 2. Typical master curve of viscoelastic behavior of viscoelastic materials with a conceptual scale of relative degree of hardness superimposed. (*RR* = rubbery region (rubbers, elastomers, e.g., Evostik and Bostik adhesives), *TR* = transition region (epoxies, e.g., Araldite 2-part epoxy), *GR* = glassy region (e.g., ceramic glues).)

In order to simplify description of the different combinations of Poisson's ratios and the Young modulus employed, the following designations are used:

RR-beam: $\nu_{ad} = 0.49999$, $E_{ad} = 0.001$ GPa, a bonded beam with adhesive properties in the rubbery region;

TR-beam: $\nu_{ad} = 0.40$, $E_{ad} = 1$ GPa, a bonded beam with adhesive properties in the rubber-to-glass transition region;

GR-beam: $\nu_{ad} = 0.30$, $E_{ad} = 10$ GPa, a bonded beam with adhesive properties in the glassy region;

H-beam: $\nu_{ad} = 0.33$, $E_{ad} = 70$ GPa, a homogeneous beam with no joint.

The Young modulus value $E_{ad} = 70$ GPa is not realistic for any polymeric structural adhesive or epoxy. It represents aluminium alloy "adhesive" which is, in fact, an aluminium alloy welding. This value was used in the analysis, in order to obtain a reference value for the maximum stresses of a single-lap adhesively bonded beam.

1.2. **Definition of Axes and Basic Equations.** As shown in Fig. 3, the components of stress in a body are defined by considering the forces acting on an infinitesimal cubical volume element whose edges are parallel with the coordinate axes 1, 2, 3 which are equivalent to the coordinates x , y , z shown in Fig. 4. As the cube is in equilibrium, the components of stress are therefore defined by six independent quantities: the normal stresses S_{11} , S_{22} , and S_{33} and the shear stresses S_{12} , S_{13} , and S_{23} .

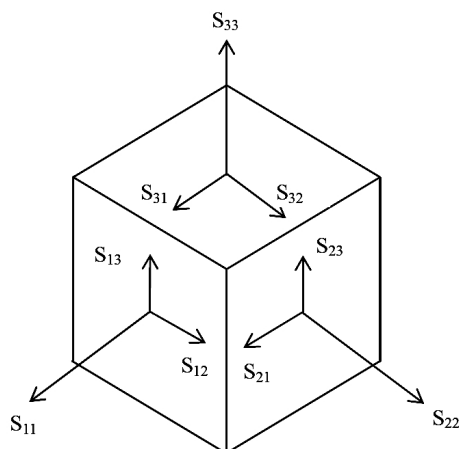


Fig. 3. Components of stresses.

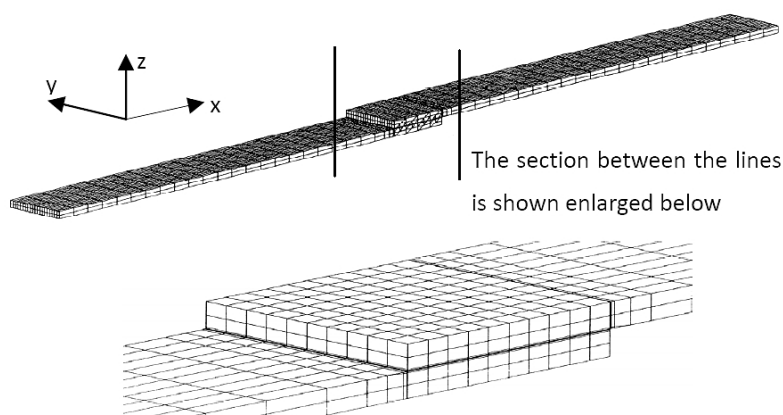


Fig. 4. Original FE mesh of the single-lap adhesively bonded beam.

1.3. **The FE Mesh.** The FE mesh was created using the ABAQUS FE pre- and post-processing program operating in X-window environment. Because of the 3D nature of the stress state in the single-lap bonded beam and because of the anticipated stress concentration in the adhesive layer of the beam, small finite elements were used within the adhesive layer and around the adhesive-adherend interfaces and larger elements were used in the outer regions of the adherends. The adhesive layer was divided into 64 equal parts along its length (x -direction) and 20 equal parts along its width (y -direction) in order to obtain an accurate indication of the variation of stresses in the lengthwise and breadthwise directions. Along the thickness (z -direction), the adhesive layer was divided into 5 equal layers of elements.

The input into the FE program was the geometrical description of 16,160 elements and their material properties. The locations of nodal points were set by the ABAQUS input file as a function of the length and width of the lap-joint beam, that is, in accordance with the geometric parameters of the model. Also the material parameters of the adhesive and adherends were input via the ABAQUS input file. The original FE mesh is shown in Fig. 4 which also shows the directions of the coordinate axes x , y , z . This model was expected to be an adequate one as it had a sufficient accuracy and a moderate number of elements [7].

2. **Effect of the Mechanical Properties of the Adhesives on Distributions of Stresses.** Since failure of single lap-joints initiates where high stresses occur, the maximum stresses are of interest. In this section, the distributions of different components of stresses along the critical line, in which the maximum stresses occur, will be studied. These investigations are carried out for 3 types of adhesives, whose properties lie within the rubbery region (RR), the rubber-to-glass transition region (TR) and the glass region (GR). Thus the investigations are based on three single-lap bonded beams, namely, RR-beam, TR-beam, and GR-beam. For purposes of comparison, the stresses induced in the homogeneous beam without a lap-joint, that is the H-beam, is also investigated.

2.1. **RR-Beam.** The original mesh and displaced mesh of the RR-beam are shown in Fig. 5. It is clear that bending is induced in both the lower and upper adherends and the adhesive layer is considerably stretched. Figure 6 shows the distributions of 6 components of stresses along the critical line along the total RR-beam. In this figure, the stress distributions in the lower adherend is indicated by dashed line, the stress distributions in the adhesive layer is indicated by solid line, and the stress distributions in the upper adherend is indicated by a dash-dotted line. It can be seen from that in the upper adherend, excepting the queer end stress concentration caused by the loading conditions, the trends of the stress distributions of the upper adherend are opposite to those of the lower adherend. However, the values of the stresses induced in the upper adherend are little bigger than those of the lower adherend as the type of support is different.

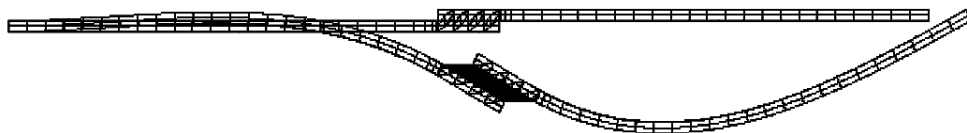


Fig. 5. Original mesh and displaced mesh of RR-beam.

2.1.1. **Variation of the Normal Stress S_{11} .** From the numerical results of the FE analyses, it was observed that the maximum value of the normal stress S_{11} occurs at the central line ($y = 0.125$ m). This means that the central line is the critical line in this case. It is seen from Fig. 6 that in the lower adherend, the value of S_{11} increases rapidly from A to B and there is a stress concentration at B . The value decreases rapidly from B and attains the minimum value near $x = 0.195$ m, then increases sharply at C . For the upper adherend,

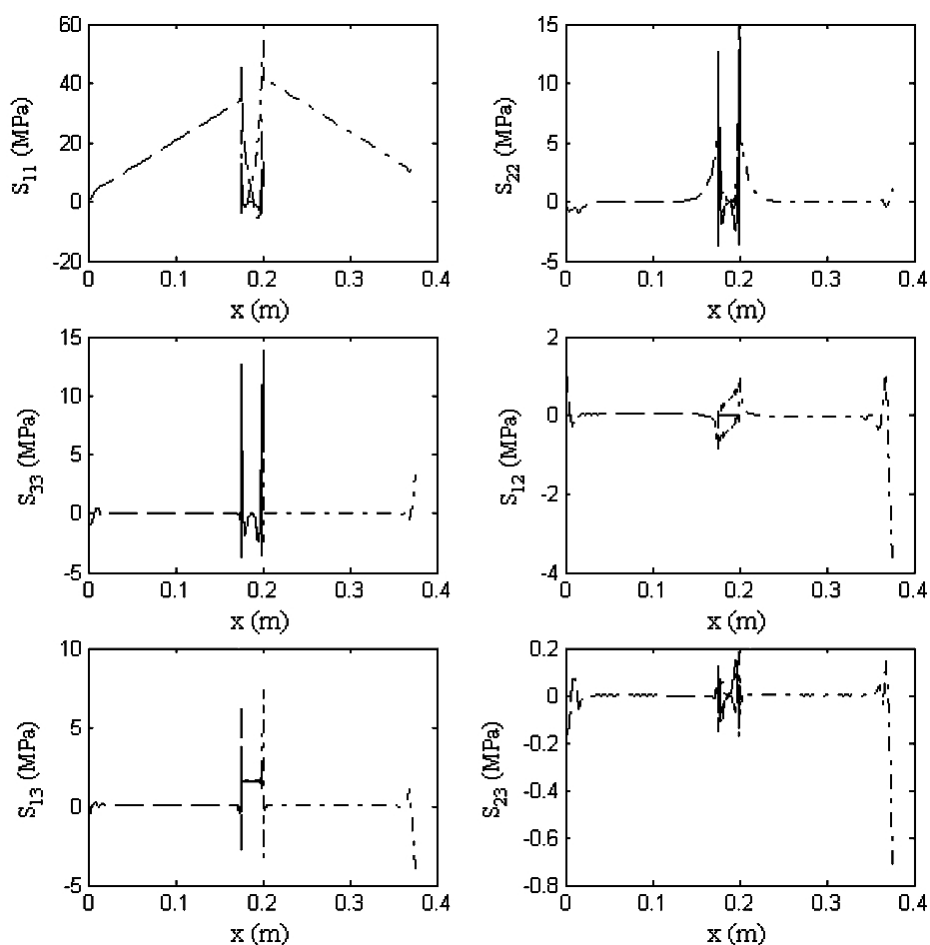


Fig. 6. Distributions of 6 components of stresses along the total RR-beam. (Designations here and in Figs. 8–10: adhesive layer = solid lines, lower adherend = dashed lines, and upper adherend = dash-dotted lines.)

the normal stress S_{11} starts at B at a magnitude which is well below the corresponding stress magnitude at location B of the lower adherend. This difference in stress magnitude is due to the load transfer provided by the adhesive, from point B , the stress in the upper adherend decreases to the minimum value at $x = 0.179$ m and then increases to the maximum value at C . Thereafter, the stress decreases until it reaches the nominal value of 10 MPa at D , the tip of the beam. This nominal value is due to the tensile load of 1000 N acting on the cross-section (25×4 mm) of the beam which is well removed from the bonded section.

In the adhesive layer, it is clear that there are stress concentrations at both the left and right free ends of the adhesive layer. However, the central region of the adhesive layer is mostly stress-free. It should be noted that for the scale of the stress variations shown in Fig. 6, the stress distribution in the adhesive layer at the lower adherend-adhesive interface and the upper adherend-adhesive interface are the same. Actually, there are very slight differences. For this loading and boundary conditions employed, the stresses in the upper interface are slightly greater than those of the lower interface. In addition, the stresses induced in the adherends at the interfaces are generally greater than those induced in the

adhesive at corresponding locations. Thus, each of the nodes located on the lower or upper interface has two different values of the same stress component. One stress component value is associated with the adherend while the other value is associated with the adhesive. These differences form a strongly pronounced stress discontinuity in the bonded section as evident from Fig. 6. This stress discontinuity may be the cause of delamination failure. This point will be discussed further in the next section.

2.1.2. *Variation of the Normal Stress S_{22}* . For the normal stress S_{22} , it is clear that the critical line is also the central line ($y = 0.125$ m). Figure 6 shows that the value of S_{22} in the lower adherend between A and B is close to zero. But near B , the value of S_{22} increases rapidly and attains the maximum value at B . Thereafter S_{22} decreases to zero but then it increases again to a high value at C . Between B and C the value of S_{22} is practically zero, but at B and C , S_{22} attains high values. There are stress concentrations at B and C . Similarly, for the upper adherend, S_{22} has high values at B and C . But between B and C , and between C and D , S_{22} is close to zero in magnitude. It is also clear that there are stress concentrations at both the left and right free ends of the adhesive layer. In addition, there is still a stress discontinuity in the bonded section, in this case, but it is less pronounced than that of the normal stress S_{11} . Furthermore, the absolute value of S_{22} is much smaller than that of S_{11} .

2.1.3. *Variation of the Normal Stress S_{33}* . As with S_{11} and S_{22} , the central line is the critical line for the normal stress S_{33} . In contrast to the distributions of S_{11} and S_{22} , in the lower adherend, Fig. 6 shows that the value of S_{33} is very close to zero from A to B but rises abruptly to the maximum value at B . Between B and C , S_{33} oscillates in value between 0 and -2 MPa. At C , S_{33} again attains the maximum value. Similarly, the values of S_{33} in the upper adherend starts from a very high value of 6 MPa at B , oscillate between 0 and -2 MPa from B to C , attain the maximum value of about 6 MPa at C and then drop abruptly to zero. Between C and D , S_{33} attains zero value. Again, there are stresses concentrations at both the free ends of the adhesive layer. Figure 6 also shows that, in the case of S_{33} , there is no significant stress discontinuity in the bonded section.

2.1.4. *Variation of the Shear Stress S_{12}* . In this case, the critical lines ($y = 0.00125$ and 0.02375 m) are very close to the front and rear edges. Figure 6 shows the rear critical line ($y = 0.02375$ m). As shown in Fig. 6, from A to B , S_{12} first keeps close to zero, then decreases near point B , and attains a low value at B . Within the bonded section, there is a slight stress discontinuity. As shown in Fig. 6, there is a high stress concentration at D , which is regarded as a result of the loading conditions.

2.1.5. *Variation of the Shear Stress S_{13}* . From the numerical results, the critical line of this case is the central line. As shown in Fig. 6, in the lower adherend, the value of S_{13} keeps close to zero from A to B and exhibits the stress concentration at B . There are stress concentrations at both free ends of the adhesive layer. In contrast to other cases, the value of S_{13} is higher than zero.

2.1.6. *Variation of the Shear Stress S_{23}* . In this case, there are two critical lines at the front and rear edges, while Fig. 6 shows the front one. From A to B , the value of S_{23} keeps close to zero and exhibits a slight stress concentration at B . Within the bonded section, the variation of S_{23} is complicated, but its value is very small. Similar to the case of S_{12} , there is a strongly pronounced stress concentration at D .

2.2. **TR-Beam**. Figure 7 shows the original mesh and displaced mesh of the TR-beam. Similar to the case of RR-beam, bending is induced in both the lower and upper adherends. In contrast to the case of RR-beam, there is not obvious stretch at the adhesive layer in this case.

The distributions of 6 components of stresses along the critical lines in the total TR-beam are shown in Fig. 8. It is clear that the variations of S_{11} , S_{22} , S_{33} , and S_{13} are similar to those of the RR-beam, but the stress values are higher than those of the RR-beam.

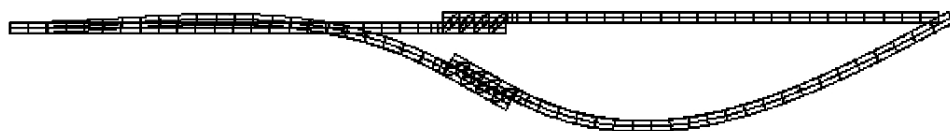


Fig. 7. Original mesh and displaced mesh of TR-beam.

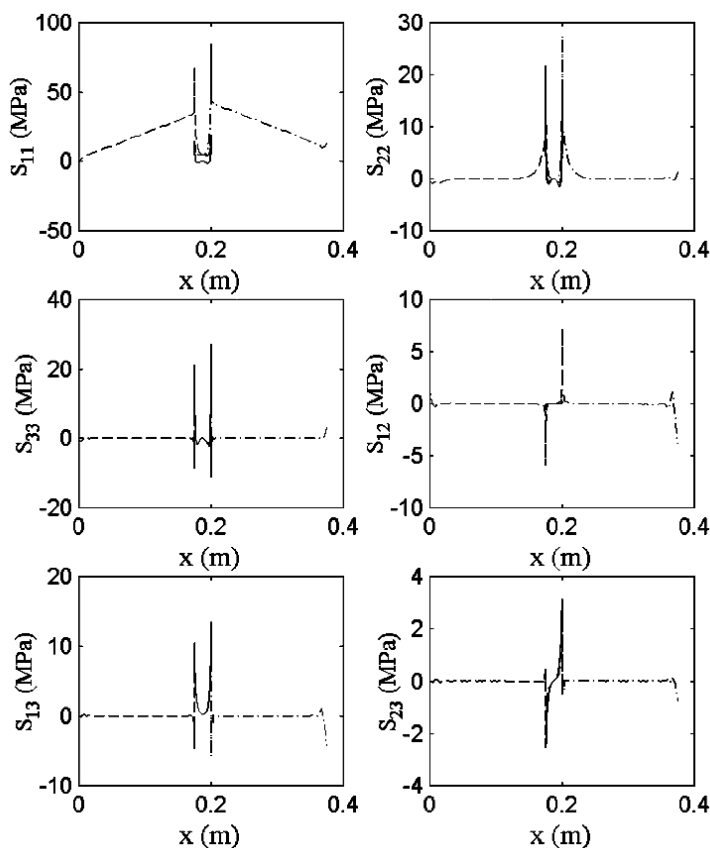


Fig. 8. Distributions of 6 components of stresses along the total TR-beam.

The stress discontinuities obviously exist only in the cases of S_{11} and S_{22} . In the cases of S_{12} and S_{23} , the variations of stresses are different from those of the RR-beam, and the values of stress concentration factors are higher.

2.3. GR-Beam. The original mesh and displaced mesh of the GR-beam are similar to the TR-beam. The distributions of 6 components of stresses along the critical lines in total GR-beam are shown in Fig. 9. It can be seen that the variations of 6 components of stresses are similar to those of the TR-beam, but the stress values are higher than in the TR-beam. The stress discontinuity obviously exists only in the case of S_{11} .

2.4. H-Beam. The original mesh and displaced mesh of the H-beam are similar to the TR-beam. Figure 10 shows the distributions of 6 components of stresses along the critical lines in total H-beam. It is clear that the variations of 6 components of stresses are similar to those of the GR-beam, but their values of the stresses are higher than in the GR-beam. As it might have been expected, there is not obvious stress discontinuity, in this case, since the H-beam is a homogeneous beam with no joints.

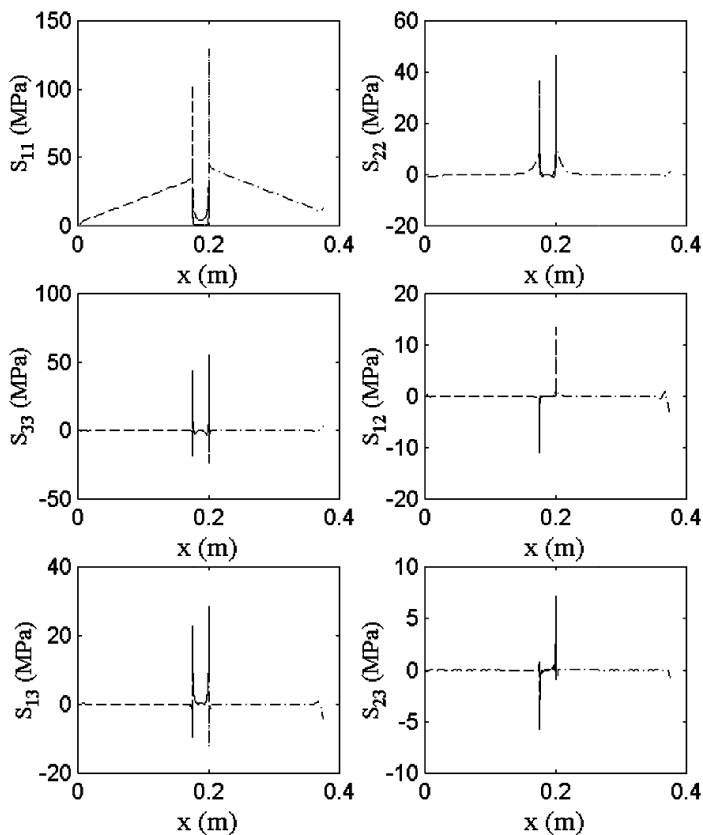


Fig. 9. Distributions of 6 components of stresses along the total GR-beam.

Among 6 components of stress, S_{11} attains the most high values, but S_{33} and S_{13} are really dangerous components, insofar as the peel is weak link of the bonded joints. The above observations imply that under the tensile loading conditions the stress field in the total single-lap adhesively bonded beams is dominated by S_{11} , S_{33} , and S_{13} .

3. Comparison of Dominating Stresses. It was shown in the previous section that for all four single-lap adhesively bonded beams the stress concentration occur at the ends of bonded section. For some of the stress components, there are stress discontinuities in the bonded section. Thus, a careful examination of the stress distributions in the bonded section is necessary. As mentioned in the previous section, the stress field in the total single-lap adhesively bonded beams is dominated by S_{11} , S_{33} , and S_{13} . The stress distributions of these dominating stress components will be discussed further.

3.1. Comparison of Normal Stresses S_{11} . Figure 11 shows the S_{11} distributions of 4 typical beams in the bonded section ($x = 0.175$ m to $x = 0.2$ m). Again, solid lines denote the stress distributions of the adhesive layer, dash lines denote the stress distributions of the lower adherend and dash/dotted lines denote the stress distributions of the upper adherend. It is seen from Fig. 11 that the stress discontinuities exist in the case of S_{11} , with exception of the H-beam, which is a homogeneous beam with no joints. The higher the hardness of adhesives, the smaller the discontinuities between the stresses induced in the adherends and adhesive at the interfaces.

Table 1 shows the values of the normal stresses S_{11} at key locations of the joint and the respective stress concentration factors, which are calculated as the ratio of the numerical

Table 1

Normal Stress S_{11} of Bonded Beams at Selected Points in the Adhesive Joint

Normal stress S_{11} (MPa)								
	RR-beam		TR-beam		GR-beam		H-beam	
Location	B	C	B	C	B	C	B	C
Adherend	45.46	54.22	67.82	84.63	103.17	129.11	158.11	197.98
Adhesive	12.70	14.40	14.81	18.93	26.33	33.15	73.99	92.71
SCF	3.58	3.76	4.58	4.47	3.93	3.89	2.14	2.14

Note. Here and in Tables 2 and 3: SCF = stress concentration factor.

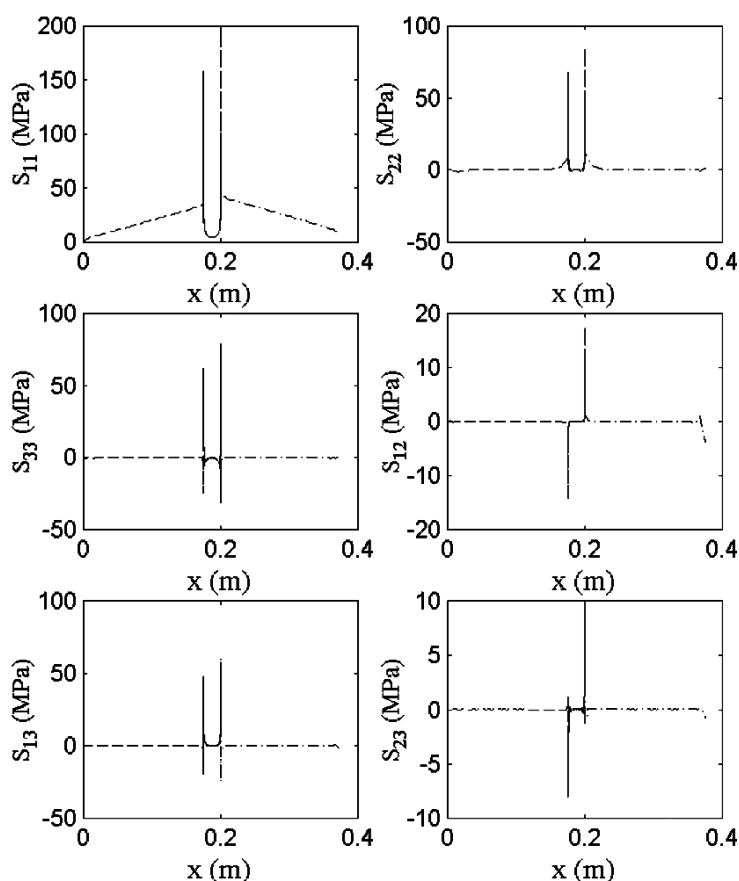


Fig. 10. Distributions of 6 components of stresses along the total H-beam.

values of stresses S_{11} in the adherend and adhesive at the same location. It is clear that, in the case of S_{11} , the stresses in adherends are much higher than in adhesives. This observation implies that the adherends sometimes are the first to fail, though they are usually stronger than the adhesives.

3.2. **Comparison of Normal Stress S_{33} .** The stress distributions of S_{33} of 4 typical beams in the bonded section are shown in Fig. 12. It can be seen that there is not stress discontinuity in this case. In contrast to the case of S_{11} , these stresses attain both positive and negative values, the absolute values of the negative ones being smaller than those of

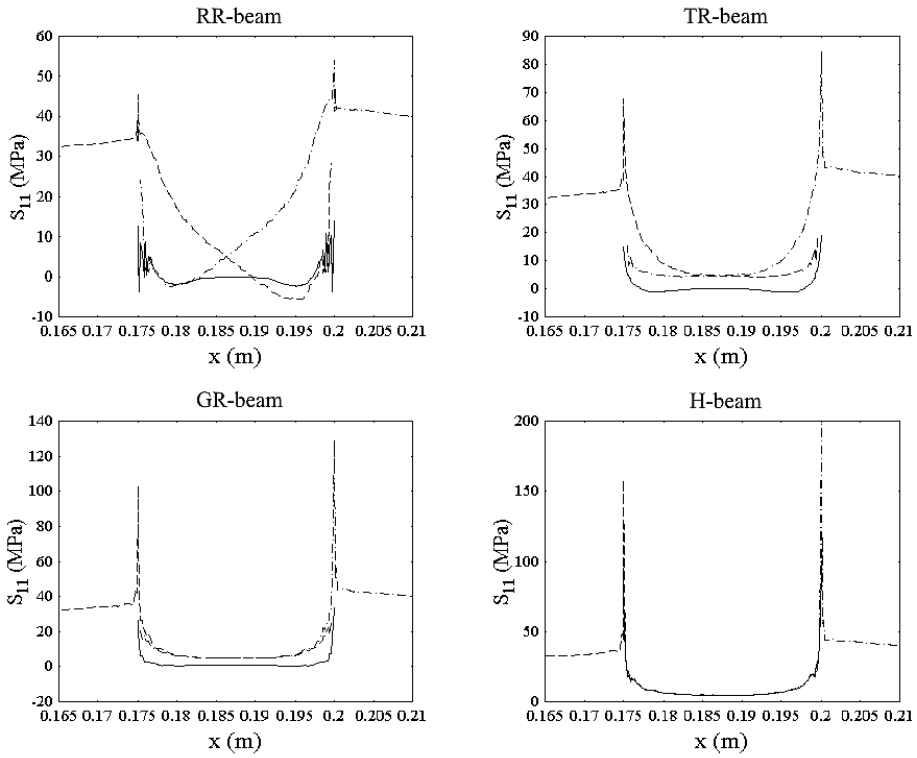


Fig. 11. Distributions of S_{11} of 4 typical beams at the bonded section.

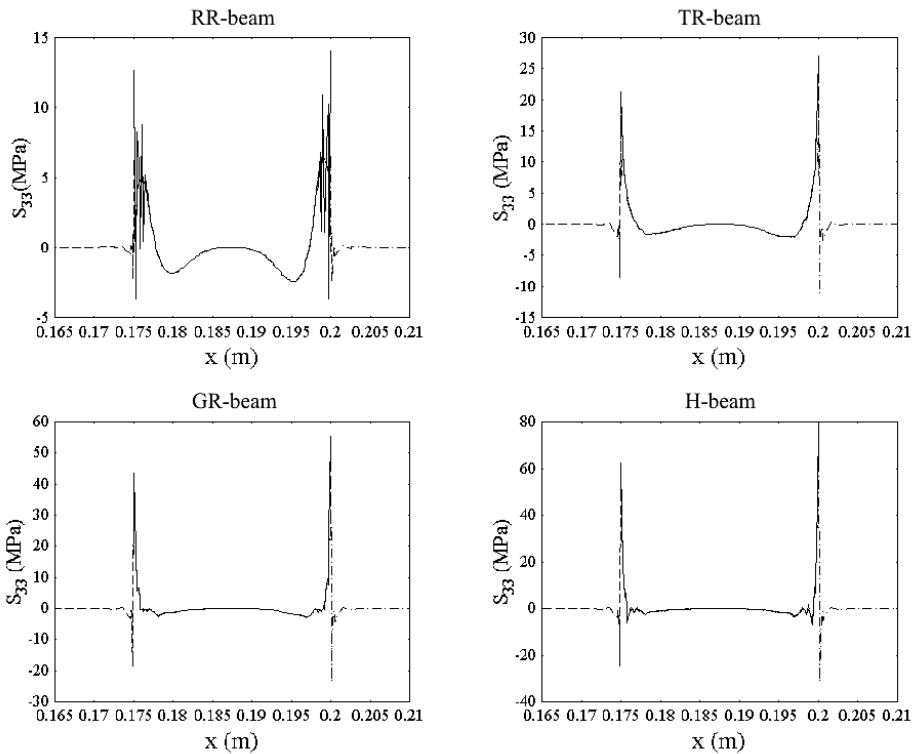
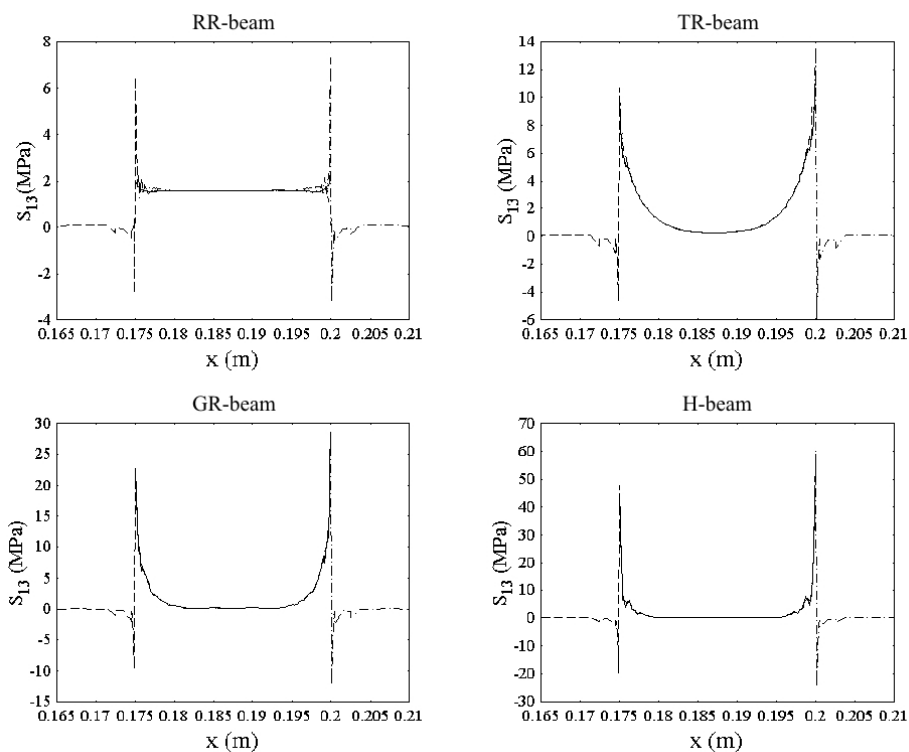


Fig. 12. Distributions of S_{33} of 4 typical beams at the bonded section.

Table 2

Normal Stress S_{33} of Bonded Beams at Selected Points in Adhesive Joint

Normal stress S_{33} (MPa)								
	RR-beam		TR-beam		GR-beam		H-beam	
Location	B	C	B	C	B	C	B	C
Adherend	6.20	6.90	15.45	19.74	33.90	42.04	55.25	69.27
Adhesive	12.70	13.90	21.17	27.10	43.49	55.35	62.08	78.83
SCF	0.49	0.50	0.73	0.73	0.76	0.76	0.89	0.88

Fig. 13. Distributions of S_{13} of 4 typical beams at the bonded section.

the positive ones. The calculated values of S_{33} at key locations of the joint and the stress concentration factors are given in Table 2. Surprisingly, all stress concentration factors are smaller than 1. In other words, in the case of S_{33} , the stresses in adhesives are higher than in adherends. This means that adhesives will certainly be the first to fail.

3.3. Comparison of Shear Stresses S_{13} . Figure 13 depicts the S_{13} distributions of 4 typical beams in the bonded section. Similar to the case of S_{33} , the calculated stresses attain both high positive values, and low negative ones. Within the bonded section, the calculated stresses values tend from positive values to zero.

Table 3 shows the numerical values of S_{13} stresses at key locations of the joint and the respective stress concentration factors. It is seen that, in the case of RR-beam, stresses in adherends are much higher than in adhesives. In the case of GR-beam, however, these values are nearly the same. It can be seen from Tables 1–3 that the stress concentration factors in the both ends of the bonded section are nearly the same.

Table 3

Shear Stress S_{13} of Bonded Beams at Selected Points in Adhesive Joint

Normal stress S_{13} (MPa)								
Location	RR-beam		TR-beam		GR-beam		H-beam	
	B	C	B	C	B	C	B	C
Adherend	7.87	7.35	10.71	13.64	22.23	28.15	47.73	60.15
Adhesive	1.95	2.07	9.44	11.84	22.74	28.49	44.87	56.11
SCF	4.04	3.55	1.13	1.15	0.98	0.99	1.06	1.07

Conclusions. The stress distributions of complete single-lap adhesively bonded beams have been investigated using the 3D FE method. Specifically, FE solutions of the stress distributions in the bonded section have been obtained for three typical characteristics of adhesives. The results are summarized as follows:

1. The stress distributions of a single-lap adhesively bonded beam are strongly affected by the characteristics of adhesive.

2. Stress discontinuities exist in the stress distributions within the adhesive and adherend at the interface, especially for the stress components S_{11} , S_{22} , S_{12} and S_{13} . The larger the hardness of adhesives, the smaller the discontinuities between the stresses induced in the adherends and adhesive at the interfaces.

3. The stress field in the total single-lap adhesively bonded beam is dominated by the normal stress components S_{11} and S_{33} , and the shear stress component S_{13} . Although the stress component S_{11} is the largest component by magnitude, but the component S_{33} is potentially more significant because it is related to the peel stress, which is ultimately responsible for the failure of adhesively bonded joints.

4. The stress concentration factors are different for various stress components, as well as various adhesives. However, the stress concentration factors in both ends of the bonded section are nearly the same.

Acknowledgment. This study is partially supported by the Special Program of the Ministry of Science and Technology, China (Grant No. 2012ZX04012-031).

Резюме

За допомогою тривимірного методу скінченних елементів досліджено розподіл напружень уздовж нерозрізних балок, адгезійно з'єднаних внапуск. Для чотирьох типових характеристик сполучних матеріалів отримано розподіл напружень у з'єднувальному перерізі. Результати досліджень показали, що для компонент напружень S_{11} , S_{22} , S_{12} та S_{13} має місце сингулярність напружень на нижній та верхній границях балки. Чим вище граничні значення твердості сполучних матеріалів, тим менше значення напружень розриву в склеюваних і сполучних матеріалах на границях. Отримані результати свідчать, що в нерозрізних балках, з'єднаних внапуск, складові нормальних S_{11} , S_{33} і дотичних S_{13} напружень є домінуючими серед складових полів напружень, при цьому напруження S_{11} є найвищим, а S_{33} – найнебезпечнішим, оскільки зв'язане з напруженням відриву. Результати чисельних досліджень проілюстрували, що коефіцієнти концентрації напружень варіюються як для різних компонент напружень, так і для різних сполучних матеріалів, проте вони практично однакові для двох кінців з'єднувального перерізу.

1. X. He, "A review of finite element analysis of adhesively bonded joints," *Int. J. Adhes. Adhesiv.*, **31**, 248–264 (2011).

2. R. D. Adams, J. Comyn, and W. C. Wake, *Structural Adhesive Joints in Engineering*, Chapman & Hall, London (1997).
3. A. Higgins, "Adhesive bonding of aircraft structures," *Int. J. Adhes. Adhesiv.*, **20**, 367–376 (2000).
4. X. He and S. O. Oyadiji, "Influence of adhesive characteristics on the transverse free vibration of single lap jointed cantilevered beams," *J. Mater. Process. Technol.*, **119**, 366–373 (2001).
5. X. He, "Study on forced vibration behavior of adhesively bonded single-lap joint," *J. Vibroeng.*, **15**, 211–218 (2013).
6. X. He, "Numerical and experimental investigations of the dynamic response of bonded beams with a single-lap joint," *Int. J. Adhes. Adhesiv.*, **37**, 79–85 (2012).
7. X. He, "Comparisons of finite element models of bonded joints," *Appl. Mech. Mater.*, **66-68**, 2192–2197 (2011).

Received 03. 09. 2013